Structure-property relationships of water adsorption in metal-organic frameworks

J. Canivet, Jonathan Bonnefoy, C. Daniel, Alexandre Legrand, Benoit Coasne, D. Farrusseng

Structure–property relationships of water adsorption in metal–organic frameworks†

Jérôme Canivet,[a] Jonathan Bonnefoy,[a] Cécile Daniel,[a] Alexandre Legrand,[a] Benoit Coasne[bc] and David Farrusseng*[a]

A set of 15 metal–organic frameworks (MIL-53, MIL-68, MIL-125, UiO-66, ZIF) exhibiting different pore size, morphology, and surface chemistry is used to unravel the numerous behaviors of water adsorption at room temperature in this class of materials. Outstanding ''S''-shaped (type V) adsorption isotherms are observed for MIL-68 type solids. We show that the underlying mechanism of water adsorption can be rationalized using a simple set of three parameters: the Henry constant (*i.e.* the slope of the adsorption pressure in the low pressure range), the pressure at which pore filling occurs, and the maximum water adsorption capacity. While the Henry constant and pore filling pressure mostly depend on the affinity of water for the surface chemistry and on pore size, respectively, these two parameters are correlated as they both reflect different aspects of the hydrophobicity–hydrophilicity of the material. For a given type of porous structure, the functionalization of the material by hydrophilic moieties such as hydrogen bonding groups (amine or aldehyde) systematically leads to an increase in the Henry constant concomitantly with a decrease in the pore filling pressure. As for the adsorption mechanism, we show that, for a given temperature, there is a critical diameter ($D_c \sim 20$ Å for water at room temperature) above which pore filling occurs through irreversible capillary condensation accompanied by capillary hysteresis loops. Below this critical diameter, pore filling is continuous and reversible unless the material exhibits some adsorption-induced flexibility.

1. Introduction

Understanding and predicting the adsorption behavior of water in microporous solids is crucial for the development of industrial processes. For instance, the temperature required for the regeneration of chromatography columns made up of molecular sieves is governed by their water adsorption properties. As a result, the hydrophilic features of zeolites are not always an advantage when one wants to capture other gases and vapors. In contrast, hyperhydrophobic zeolites can be applied for molecular springs upon water intrusion.[1] Of particular importance for environmental applications, water adsorption is often detrimental for CO_2 capture using hydrophilic materials since water acts as a strong competitor. In contrast, it was demonstrated that controlled water adsorption can enhance CO_2 capture in MOFs[2] such as MOF-100,[3] HKUST-1,[4] MIL-101[5] and MIL-53.[6] As a last example, microporous adsorbents with controlled hydrophilicity are being developed for cooling and heat pump systems.[7] The conventional silica-gel–water adsorption systems are not very energy efficient since most of the water adsorption occurs outside operating pressure windows.

Kaskel and coworkers have reported that water adsorption on a series of MOFs, namely HKUST-1, ZIF-8, MIL-101(Cr), and MIL-101(Fe), displays a broad variety of behaviors.[8] The mesoporous MIL-100/-101 show an exceptional water capacity of ~ 1 g g^{-1} while the water affinity for the other materials ranges from hydrophilic (HKUST-1) to very hydrophobic MOF (ZIF-8). More recently, Walton and coworkers have reported water adsorption isotherms for another series of MOFs including UiO-66, Mg-MOF-74, DMOF-1 and UMCM-1 and compared them with reference micro-mesoporous materials.[9] The large water capacity of MIL-100/-101 associated with an adsorption isotherm exhibiting a combination of type I and type V isotherms[10] makes these materials of particular interest for adsorption-based cooling and heat pumps.[7e] Such adsorption isotherms are made up of two steps which can be described as follows. The first step (concave adsorption isotherm) is related

[a] *IRCELYON, Université Lyon 1, CNRS, UMR 5256, 2 avenue Albert Einstein, F-69626 Villeurbanne, France. E-mail: david.farrusseng@ircelyon.univ-lyon1.fr; Fax: +33 4 72 44 53 99; Tel: +33 4 72 44 53 65*

[b] *MultiScale Material Science for Energy and Environment, CNRS/MIT (UMI 3466), Massachusetts Institute of Technology, 77 Massachusetts Avenue, Cambridge MA 02139, USA*

[c] *Department of Civil and Environmental Engineering, Massachusetts Institute of Technology, 77 Massachusetts Avenue, Cambridge MA 02139, USA*

† Electronic supplementary information (ESI) available: Characterization of (Ga) MIL-53-NH_2 and the correlation between the morphological properties of MOFs and their nitrogen or water adsorption capacity. See DOI: 10.1039/c4nj00076e

to the adsorption at the inorganic clusters and corresponds to type I adsorption. The second step (which is also concave) is related to the filling of mesoporous cavities and corresponds to a type V adsorption. Kitagawa and coworkers have investigated the effect of linker functionalization on water adsorption.[11] The degree of hydrophilicity, which can be assessed from the water partial pressure at which pore filling occurs, is significantly modified when the terephthalate linker is functionalized with $-NH_2$, $-NO_2$ or $-SO_3H$. Such functionalization effects have been observed for other carboxylate-based MOFs such as UiO-66[12] and ''azolate'' type MOFs which also show water uptake fine tuning.[13] The effect of linker functionalization on the breathing properties of MIL-53 (Al, Fe), MIL-88, and CID-5/6 upon water uptake has also been reported.[14]

From a qualitative point of view, the adsorption properties of MOFs are obviously quite diverse in terms of water uptake capacity, pressure at which pore filling occurs, and shape of the adsorption isotherm. Although the effect of pore functionalization has been already reported,[11,13,15] the effects of pore size, morphology, and flexibility on water adsorption have not been investigated in a systematic fashion. The lack of a comprehensive and predictive model of water adsorption is hence limiting the design of MOFs for applications where water is involved. In the present work, we report water adsorption isotherms for a large set of 15 different MOFs which were selected as they are known to be stable in moisture. We show that the adsorption behavior of water in MOFs depends mostly on the pore morphology and size while the chemical nature of the linker allows fine tuning of the hydrophilicity of the host material.

2. Experimental details

2.1. Metal–organic framework library

Fifteen different MOFs were selected in order to cover a wide range of structural features which are expected to play a key role in the adsorption properties of the host material. The library of MOF structures that has been selected is described in Table 1. Porous structural variables include pore size, pore window size, pore volume, pore structure dimension (3D cavity *versus* 1D channel), surface decoration by functional groups, and possibility of adsorption-induced breathing. The porous structures of the selected MOFs are depicted in Fig. 1. The selection of MOFs covers broad ranges of pore size and of pore window, from 6 to 34 Å and 3 to 15 Å, respectively. Porous solids based on MIL-101, UiO-66, MIL-125 and ZIF-8 structures exhibit a 3D type pore structure. MIL-101 and UiO-66 show two types of cavities of diameter 29 and 34 Å and 7.5 and 11 Å, respectively. The MIL-125 structure also corresponds to the 3D arrangement of two types of cages with effective accessible diameters of 12.5 and 6 Å. SIM-1 is isostructural to ZIF-8, *i.e.* it has the same SOD structure, but is constructed from 3-methyl-4-carboxy-imidazolate linkers. Because the substituents on the imidazolate linker point toward the center of the cavity, the pore size and pore volume of SIM-1 are smaller than those of ZIF-8. The other solids of the library have a 1D channel porous structure. On one hand, MIL-68 is made up of triangular and hexagonal channels of diameters 6 and 16 Å, respectively. On the other hand, MIL-53 is made up of a diamond type channel which can adopt different openings depending on the structure flexibility.

Keeping the porous structure identical, the decoration of the walls by polar groups has been carried out systematically in order to assess the effect of additional hydrogen bonding on the adsorption properties of water. While the water adsorption capacity can be easily measured as the uptake at partial pressure close to the bulk saturating vapor pressure p°, the evaluation of the surface hydrophilicity is not straightforward. Indeed, the hydro-lipophilicity balance for porous solids is more a concept than an actual property that can be assessed easily. In the present work, we consider three quantitative indicators of hydrophilicity–hydrophobicity that can be estimated from water adsorption data. The first indicator is the Henry constant, K_H, which corresponds to the slope of the adsorption isotherm at very low water partial pressures (where the adsorbed amount increases linearly with water pressure). The second indicator is the relative pressure $\alpha = p/p^\circ$ at which half of the total water capacity is reached; α decreases with increasing ''hydrophilicity'' of

Table 1 MOF library considered in the present work

#	Name	Surface area[a] ($m^2\ g^{-1}$)	Pore volume[a] ($cm^3\ g^{-1}$)	Pore size (Å)	Window size (Å)	Pore structure	Possibility of breathing	Surface decoration
1	Cr-MIL-101	2500	1.22	29 & 34	12 & 15	3D	No	None
2	Cr-MIL-101-NH_2	1790	0.97	29 & 34	12 & 15	3D	No	$-NH_2$
3	Cr-MIL-101-NO_2	2040	0.95	29 & 34	12 & 15	3D	No	$-NO_2$
4	Zr-UiO-66	1030	0.40	7.5 & 11	4 & 6	3D	No	None
5	Zr-UiO-66-NH_2	830	0.35	7.5 & 11	4 & 6	3D	No	$-NH_2$
6	Ti-MIL-125	1160	0.47	6 & 12	5	3D	No	None
7	Ti-MIL-125-NH_2	1230	0.51	6 & 12	5	3D	No	$-NH_2$
8	ZIF-8	1530	0.48	11	3 & 5	3D	No	None
9	SIM-1	570	0.30	6.5	n.d.	3D	No	–CHO
10	Al-MIL-53	1040	0.51	7 to 13	n.a.	1D	Yes	None
11	Al-MIL-53-NH_2	940	0.37	7 to 13	n.a.	1D	Yes	$-NH_2$
12	Ga-MIL-53	1230	0.47	8 to 20	n.a.	1D	Yes	None
13	Ga-MIL-53-NH_2	210	n.d.	8 to 20	n.a.	1D	Yes	$-NH_2$
14	In-MIL-68	1100	0.42	6 & 16	n.a.	1D	No	None
15	In-MIL-68-NH_2	850	0.30	6 & 16	n.a.	1D	No	$-NH_2$

[a] Determined from the N_2 adsorption isotherm at 77 K, n.a. not applicable, n.d. not determined.

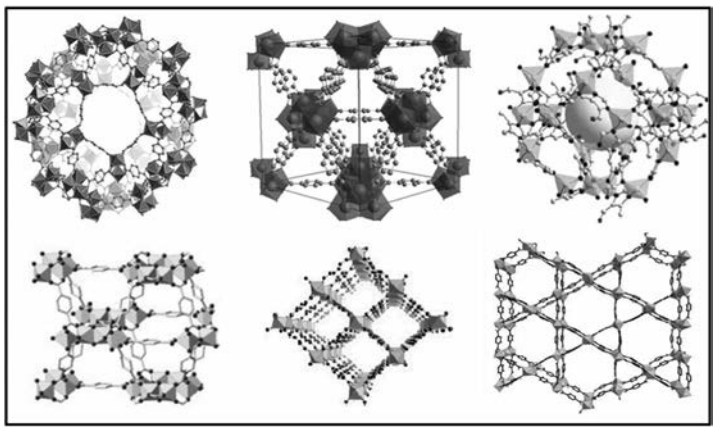

Fig. 1 Scheme of pore topologies for the different MOFs. Upper line, from left to right, MIL-125, UiO-66, SIM-1. Bottom line, from left to right, MIL-125, MIL-53, MIL-68.

the porous solid. The advantages of this dimensionless indicator are that (1) it is independent of the water adsorption capacity and (2) it is normalized ($0 < \alpha < 1$) upon exception of super-hydrophic ultramicroporous zeolites for which water adsorption proceeds by liquid water intrusion ($\alpha > 1$). The third indicator is the water adsorption capacity C_{H_2O} (in cm^3 of water per g of the sample).

2.2. Synthesis

The powder samples of Cr-MIL-101-NO_2 and –NH_2,[16] Ti-MIL-125 and Ti-MIL-125-NH_2,[17] Zr-UiO-66 and Zr-UiO-66-NH_2,[18] SIM-1,[19] ZIF-8,[20] Al-MIL-53,[21] Al-MIL-53-NH_2,[22] In-MIL-68,[23] In-MIL-68-NH_2,[24] and Ga-MIL-53[25] have been prepared according to methods published elsewhere. The synthesis of Ga-MIL-53-NH_2 is reported for the first time. Gallium nitrate (5 mmol, 1.279 g) and 2-amino terephthalic acid (5 mmol, 0.906 g) were dissolved in a solution of THF/water (1/1). Upon adding Et_3N (1.223 ml, 10 mmol) dropwise, a yellow solid precipitated instantaneously. The solid was washed 3 times with fresh THF–water solution and finally with a THF soxhlet for one day before drying under vacuum at room temperature. Ga-MIL-53-NH_2 has been left 2 days in boiling water and heated at 170 °C without decrease of crystallinity. Powder X-Ray Diffraction patterns can be found in Fig. S1 in the ESI.† The stability under humid conditions of MIL-101,[8] MIL-53,[26] ZIF-8,[20] SIM-1,[27] UiO-66[9] and Ti-MIL-125[28] can be found elsewhere (see also ref. 29 for a theoretical discussion on the stability of MOF in water).

2.3. Characterization

Powder X-ray diffraction (XRD) patterns were recorded on a Brücker D5005 apparatus. For all samples, the diffractograms indicate pure phases. The nitrogen adsorption–desorption isotherms were measured at 77 K on a BelMini device (BelJapan). The specific surface areas were calculated by the BET method. The water adsorption isotherms were measured at 298 K on a BelMax system (BelJapan). Typically, the cell was loaded with 10–50 mg of samples which were outgassed for 12 h at 413 K under secondary vacuum. Adsorption equilibrium was assumed when the variation of cell pressure was 0.3% lower for a minimum period of 300 s. This relative equilibrium criterion, which was optimised using zeolite and carbon standard samples, results in a measurement duration of 2 to 3 days per sample. Adsorption measurements were stopped at $p/p^\circ = 0.9$ in order to limit inter-crystalline water condensation ($p^o_{298K} = 3.16$ kPa). In what follows, the water uptake is reported in g of water adsorbed per g of the dried sample as a function of p/p° which corresponds to the relative humidity at 298 K. The Henry constant K_H, which characterizes the affinity of water for the surface chemistry of the MOFs, is calculated by linear regression of the adsorption isotherms for $p/p^\circ < 0.1$ (usually using 5 data points and at least 3 data points).

3. Results

The water adsorption isotherms of the MIL-101 series exhibit two distinct steps (Fig. 2). As described in the Introduction, such adsorption isotherms exhibit a combination of type I and type V isotherms.[10] The first step is related to the adsorption at the inorganic clusters and corresponds to type I adsorption while the second step (which is also concave) is related to the filling of mesoporous cavities and corresponds to a type V adsorption. The total capacity of ~ 0.9 g g^{-1} is in line with the total porous volume as already indicated by Janiak and coworkers.[29] As first suggested by Kitagawa and coworkers, we propose that adsorption at the lowest pressure ($p/p^\circ < 0.2$) corresponds to adsorption at or near the inorganic clusters while the two abrupt uptakes at higher pressures consist of filling of the two distinct mesoporous cavities of 29 and 34 Å. Given the irreversibility of the two uptakes at high pressures (*i.e.* hysteresis phenomena), we assume that pore filling occurs through capillary condensation. This result is consistent with the fact that, for water at room temperature, the pore diameter below which pore filling becomes reversible is about the critical diameter $D_c = 20$ Å. This value was estimated from the following formula which has been shown to describe both

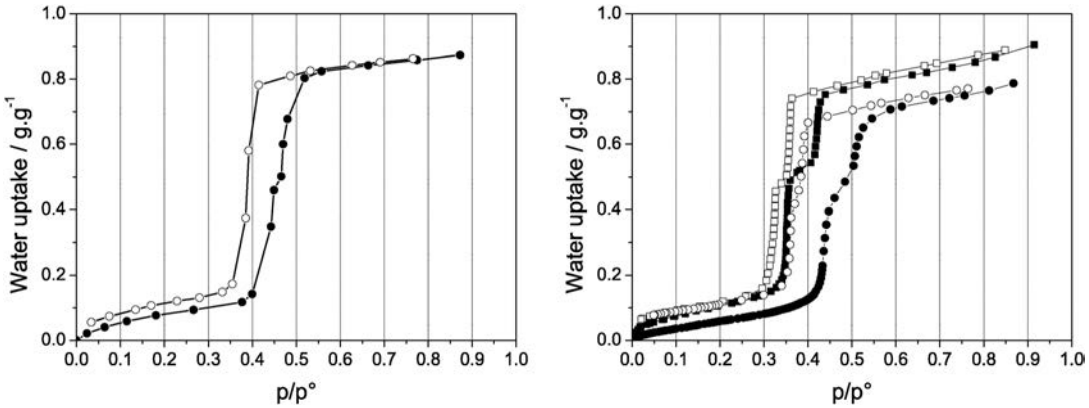

Fig. 2 Water adsorption isotherms at 298 K of (left) Cr-MIL-101; Cr-MIL-101-NH_2 (square) and Cr-MIL-101-NO_2 (circle); (right). The full and empty symbols are the adsorption and desorption branches, respectively.

molecular simulations and experiments on adsorption in porous materials:[30]

$$D_c = 4\sigma T_c/(T_c - T) \quad (1)$$

where σ = 2.8 Å is the size of the water molecule, T is the temperature, and T_c = 647 K is the bulk critical temperature for water.

The vapor pressure α at which condensation occurs can be tuned by modifying the surface decoration of the linker in MOF. The pore filling pressures for Cr-MIL-101, Cr-MIL-101-NO_2 and Cr-MIL-101-NH_2 are α = 0.47, 4.45 and 0.35, respectively. The larger hydrophilicity for Cr-MIL-101-NH_2 with respect to pristine MIL-101 and Cr-MIL-101-NO_2 is in good agreement with earlier work in which larger adsorption enthalpy was reported for the former.[11] Interestingly, water desorption takes place at very similar pressure for all MIL-101, p/p° = 0.37 ± 0.02. Consequently, the hysteresis loops are wider for Cr-MIL-101 and Cr-MIL-101-NO_2 than those for Cr-MIL-101-NH_2. These observations can be understood as follows. Because of its larger surface hydrophilicity, water adsorption prior to capillary condensation in Cr-MIL-101-NH_2 is larger than in the two other materials. At p/p° = 0.3, the amount of water adsorbed in Cr-MIL-101-NH_2 is approximately twice that in Cr-MIL-101-NO_2. As a result, the cavity (corresponding to the pore volume less than the volume occupied by the adsorbed water molecules) that gets filled upon capillary condensation is smaller for Cr-MIL-101-NH_2 than for Cr-MIL-101 and Cr-MIL-101-NO_2. In turn, because of its smaller size, such a cavity fills at a lower capillary condensation pressure than for the other materials. In contrast, the desorption pressures for these three materials are very similar; this is due to the fact that, since the sizes of the fully filled pore are very similar, desorption takes place at the similar pressure.

In contrast to the "S" shape of the water adsorption isotherms of the MIL-101 series, the water uptake on UiO-66 solids is rather continuous in the low pressure range (Fig. 3). The absence of significant hysteresis loops for the UiO-66 solids supports the assumption that capillary condensation does not take place in these materials and is replaced by reversible continuous pore filling. The absence of capillary condensation for the UiO-66 solids is consistent with the discussion above on the pseudo critical point of confined water; at room temperature, pore filling by water occurs through capillary condensation for pore sizes larger than D_c = 20 Å and through reversible continuous filling otherwise. We suggest that the minor irreversibility (*i.e.* the adsorption and desorption branches do not

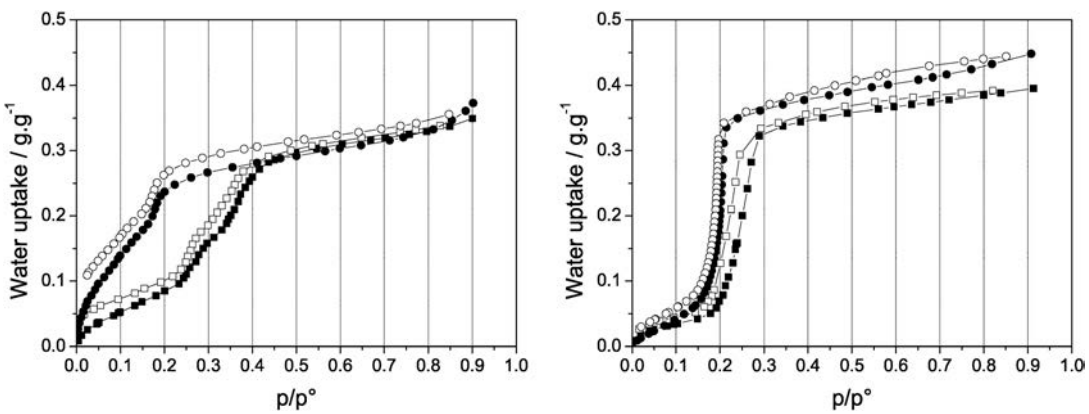

Fig. 3 Water adsorption isotherms at room temperature of: (left) Zr-UiO-66 (square) and Zr-UiO-66-NH_2 (circle); (right) Ti-MIL-125 (square) and Ti-MIL-125-NH_2 (circle). The full and empty symbols correspond to the adsorption and desorption branches, respectively.

Table 2 Adsorption data derived from N_2 adsorption isotherms at 77 K and water adsorption data at 298 K

#	MOF	BET surface[a] ($m^2\ g^{-1}$)	Volume[a] ($cm^3\ g^{-1}$)	Water capacity[b] ($cm^3\ g^{-1}$)	α	K_H[c] (mol g^{-1} Pa^{-1})	Log (K_H)
1	Cr-MIL-101	2500	1.22	0.87	0.47	9.68×10^{-06}	−5.0
2	Cr-MIL-101-NH_2	2080	0.973	0.90	0.35	4.05×10^{-05}	−4.4
3	Cr-MIL-101-NO_2	2000	0.95	0.70	0.45	5.03×10^{-06}	−5.3
4	Zr-UiO-66	1030	0.405	0.36	0.33	3.52×10^{-04}	−3.5
5	Zr-UiO-66-NH_2	830	0.35	0.36	0.15	4.1×10^{-03}	−2.4
6	Ti-MIL-125	1160	0.47	0.36	0.25	2.75×10^{-04}	−3.6
7	Ti-MIL-125-NH_2	1230	0.51	0.36	0.20	3.10×10^{-4}	−3.51
8	ZIF-8	1530	0.485	0	0.9	5.70×10^{-07}	−6.2
9	SIM-1	570	0.303	0.14	0.27	1.33×10^{-06}	−5.9
10	Al-MIL-53	1040	0.51	0.09	0.14	1.17×10^{-06}	−5.9
11	Al-MIL-53-NH_2	940	0.37	0.08	0.04	2.16×10^{-05}	−4.67
12	Ga-MIL-53	1230	0.47	0.05	0.02	1.26×10^{-05}	−4.90
13	Ga-MIL-53-NH_2	210	n.d.	—	0.02	2.32×10^{-05}	−4.63
14	In-MIL-68	1100	0.42	0.32	0.58	2.53×10^{-07}	−6.6
15	In-MIL-68-NH_2	850	0.302	0.32	0.44	1.17×10^{-06}	−5.9

[a] Estimated from N_2 adsorption isotherms at 77 K. [b] At relative humidity p/p° = 0.9. [c] 10% experimental error.

match perfectly) arises from a weak flexibility of the framework (for a recent perspective article on adsorption-induced deformation of MOF, see ref. 31). In a similar manner, we anticipate a guest–host interaction for the UiO solids since the benzene ring could be orientated differently in order to increase the interaction with water molecules. The uptakes observed in the water adsorption isotherms of the UiO solids are thought to correspond to the filling of the two different pore sizes present in the UiO structure. The amino and non-amino derivatives of the UiO solid exhibit the same water capacity of 0.35 g g^{-1}. On the other hand, the amino decoration makes the solid more hydrophilic as indicated by both the partial pressure at which half of the capacity is attained (α = 0.33 for Zr-UiO-66 against α = 0.15 for Zr-UiO-66-NH_2) and the Henry constants ($K_H = 3.5 \times 10^{-4}$ mol g^{-1} Pa^{-1} for Zr-UiO-66 against $K_H = 4.1 \times 10^{-3}$ mol g^{-1} Pa^{-1} for Zr-UiO-66-NH_2).

The interpretation of the water adsorption isotherms of Ti-MIL-125 resembles that of the UiO-66 series. Moreover, K_H and α are in the same order for these four materials (Table 2, entries #4 to #7). These results were expected since these solids exhibit relatively similar pore size and surface chemistry (Table 1).

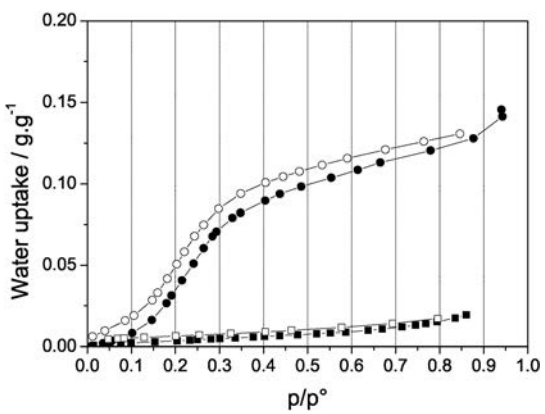

Fig. 4 Water adsorption isotherms at room temperature of ZIF-8 (square) and SIM-1 (circle). The full and empty symbols correspond to the adsorption and desorption branches, respectively.

ZIF-8 does not show significant water uptake below the relative pressure of α = 0.9 (Fig. 4). This hydrophobic feature of ZIF-8 was previously reported by Kaskel and coworkers.[8] In contrast, significant water uptake is observed when the ZIF inner surface is functionalized by accessible aldehyde groups, *i.e.* SIM-1, for which an "S" shape adsorption isotherm is obtained. Interestingly, the water–solid interactions are very weak at low relative pressure as indicated by the low Henry constants ($K_H < 10^{-6}$ mol g^{-1} Pa^{-1}) which can be an asset for gas separation under partially dried conditions (*i.e.* less than 10% of relative humidity[32]). Such a hydrophobicity arises from the absence of hydrogen bond groups at the surface of the porous material and uncoordinated centers from the inorganic pattern.

The water adsorption isotherm of Al-MIL-53 has an "S" shape with a single adsorption step which takes place at the relative pressure α = 0.15 (Fig. 5). The desorption occurs at a pressure lower than adsorption so that a hysteresis loop appears. In contrast, the water uptake of Al-MIL-53-NH_2 follows a type-I adsorption isotherm such as found in hydrophilic zeolites. It is characterized by a sharp adsorption at low pressure followed by a large plateau at saturation. Another difference between the Al-MIL-53 series is the reversibility of the desorption phenomenon for Al-MIL-53-NH_2. It is acknowledged that Al-MIL-53-NH_2 is much less flexible than Al-MIL-53 because of internal H-bonding between the bridging OH and $-NH_2$ moieties.[33] We believe that the irreversibility of the adsorption isotherm in the case of Al-MIL-53 arises from its greater flexibility upon adsorption.

Ga-MIL-53 is isoreticular to Al-MIL-53. The structure is known to be relatively rigid since the large pore structure is obtained by heating at 220 °C against 60 °C for its Al counterpart.[25a,34] The water adsorption isotherms of Ga-MIL-53 show a type-I isotherm similar to Al-MIL-53-NH_2 which reflects the framework rigidity upon adsorption (no hysteresis). The adsorption isotherm of Ga-MIL-53-NH_2 is more complex to interpret. The rather continuous increase in the water uptake upon increasing the pressure may have two different origins. It might indicate that adsorption proceeds through multilayer

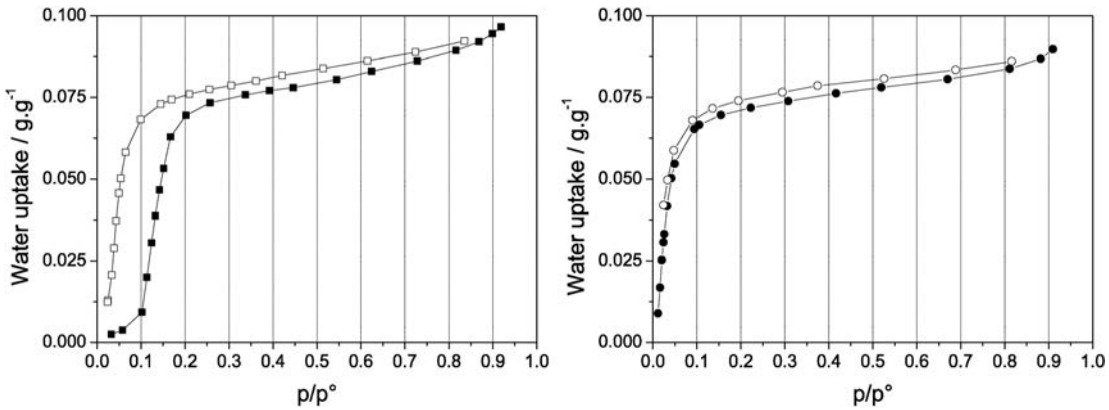

Fig. 5 Water adsorption isotherms at 298 K of: Al-MIL-53 (left); Al-MIL-53-NH_2 (right). The full and empty symbols correspond to the adsorption and desorption branches, respectively.

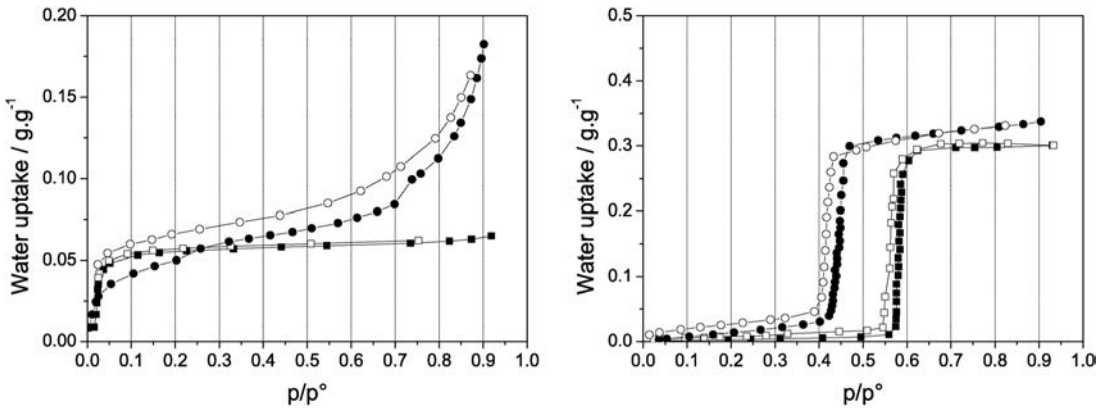

Fig. 6 Water adsorption isotherms at room temperature of: (left) Ga-MIL-53 (square) and Ga-MIL-53-NH_2 (circle); (right) In-MIL-68 (square) and In-MIL-68-NH_2 (circle). The full and empty symbols correspond to the adsorption and desorption branches, respectively.

adsorption in mesoporous and/or macroporous defects followed by capillary condensation. Given the large pressure at which the latter phenomenon is observed, we believe that it occurs in the voids between the crystallites. This hypothesis is consistent with the N_2 adsorption isotherm at 77 K which shows major uptake at relatively high pressure corresponding to macropores (Fig. S2 in the ESI†). Gate opening cannot be ruled out although CO_2 adsorption at high pressure does not reveal such a phenomenon (Fig. S3, ESI†).

In-MIL-68 based adsorbents show well-defined "S"-shaped water adsorption isotherms (Fig. 6). Such adsorption isotherms, which are referred to as Type V in the IUPAC classification, are observed when the fluid–solid interaction is weak compared to the fluid–fluid interaction such as for the adsorption of water on some activated Carbons.[11] In this case, the isotherm is convex at low pressure, reflecting the growing effect of fluid–fluid interactions before reaching an inflection point where the isotherm adopts a concave shape as it approaches saturation. Below the relative pressure α at which pore filling occurs, the adsorbent is almost evacuated. This profile is usually observed for hydrophobe activated carbon.[35] The large hydrophobicity of In-MIL-68 (α = 0.58) is surprising as we expected uptake at lower pressure because of H-bonding between water and the –OH bridging groups of the In(O)(OH) inorganic chain. We suspect that this "Dirac"-type profile arises from the one dimensional channel structure of the MIL-68 associated with relative large micropore opening (16 Å). As expected for this pore size (see discussion above on the existence of a pseudo critical capillary temperature in porous materials), the adsorption isotherms are reversible as the pore size is smaller than the critical diameter of 20 Å while the very narrow observed hysteresis is believed to be due to minor flexibility upon adsorption. As in the case of the adsorbents discussed above, the functionalization of the walls with $-NH_2$ (*i.e.* hydrophilic) groups leads to a decrease in the pore filling pressure (α = 0.44 instead of 0.57 for pristine In-MIL-68).

The morphological features obtained from N_2 and water adsorption are reported in Table 2. We can observe correlations between the different morphological parameters estimated from adsorption data, *i.e.* surface area, total porous volume, and total water capacity (Fig. S3, ESI†). Obviously, the porous volume and surface area calculated from the N_2 adsorption isotherms are very well correlated. We note a statistical deviation of the porous volume data of MIL-101 solids which are apparently slightly overestimated. As expected, the total adsorption capacities of water and N_2 agree. In addition to minor deviations for MIL-101 solids, we can observe major pitfalls for MIL-53 and ZIF adsorbents

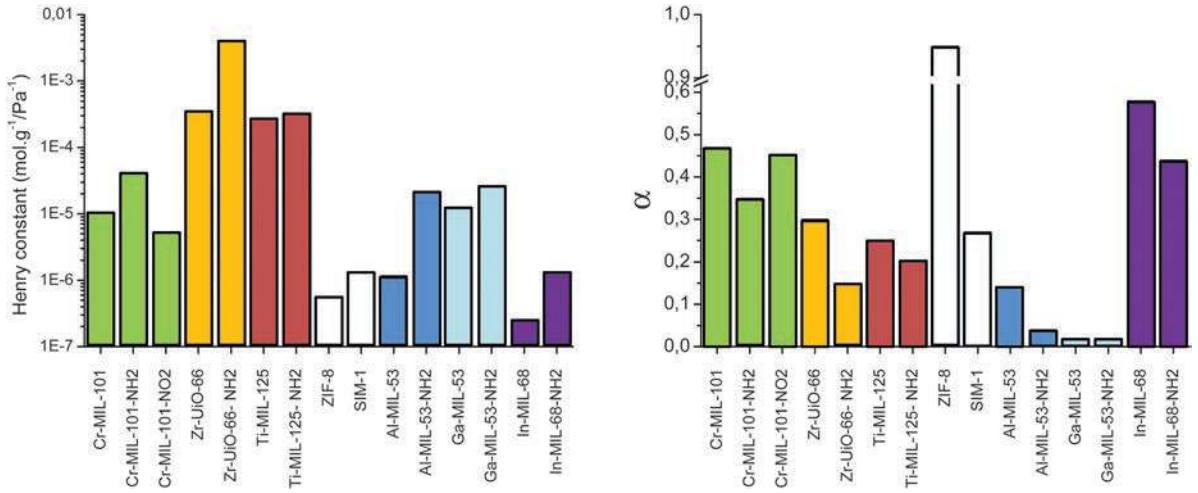

Fig. 7 Henry constants K_H measured for water at $p/p^\circ < 0.1$ (left); relative pressure $\alpha = p/p^\circ$ at which half of the maximum water uptake is reached (right).

which originate from different mechanisms. In the case of MIL-53 samples, the structural flexibility of the host matrix upon water adsorption is responsible for the very low water adsorption capacity; while the porous volume is measured for the most open forms of the MIL-53, shrinkage of the porous structure upon water adsorption likely takes place for all MIL-53. Such guest–host interactions are well established for water–Al-MIL-53[36] and CO_2–Al-MIL-53(NH_2).[33a] As a consequence, the total adsorption capacities measured with different probe molecules may not match for flexible MOFs. The large hydrophobicity associated with a small cage window is the reason for the mismatch between water and N_2 total capacities in the case of ZIF-8. Indeed, ZIF-8 does not adsorb water in their microporous cages even at pressures close to the bulk saturating vapor pressure. This property is well known for silicalite-1,[37] dehydroxylated silica[38] and, in general, for hyperhydrophobic small zeolites for which an intrusion pressure must be applied to force water to penetrate the porous network.[39]

The difference of water uptakes at low pressure is well captured by the Henry constants K_H (Fig. 7). For the same material morphology and pore size (such as in the MIL-101 series), K_H mainly depends on the surface chemistry. Henry constants K_H of water adsorption in MOFs materials span over four orders of magnitude from 5.7×10^{-7} to 4.1×10^{-3} for ZIF-8 and Zr-UiO-66-NH_2, respectively (Table 2). This broad range of Henry constants reveals the large difference of surface properties of the MOF library. The decoration of the terephthalate linker by an amino group systematically increases Henry constants K_H; the largest enhancement being for UiO-66 with an increased Henry constant by more than 10 fold (Fig. 7). Similarly, we observe a high diversity of the α values from 0.02 to 0.9 for Ga-MIL-53 and ZIF-8, respectively. The decoration of the MOF surface with polar functions systematically leads to a decrease in α, *i.e.* increase in the hydrophilicity of the material. We note that, depending on the adsorption isotherm type, K_H may probe different regimes. For hydrophobic samples such as MIL-68, ZIF-8, and SIM-1, K_H is representative of the non wetting behavior of the material as pore filling starts at $p/p^\circ > 0.1$. In contrast, for hydrophilic samples, K_H probes in part the filling of the material porosity so that these Henry constants are necessarily larger than those for hydrophobic samples. Consequently, the range of values of K_H for the different samples (*i.e.* hydrophobic *versus* hydrophilic) makes this simple indicator a very powerful tool to compare different MOFs.

4. Discussion

As far as the type of filling mechanism is concerned, we have already discussed that eqn (1) allows us to predict from the pore/cavity size if pore filling occurs through capillary condensation or reversible continuous filling. Interestingly, the critical pore size D_c below which capillary condensation is replaced by continuous and reversible filling is independent of the hydrophobicity. This result is in agreement with molecular simulations in which it was found that, for a given temperature, adsorption of wetting fluids and intrusion of non-wetting fluids become reversible at similar pore diameters.[40] Isosteric heats of adsorption were already reported for Cr-MIL-101[29,41] and MIL-100.[42] At low coverage ($p/p^\circ < 0.1$), the isosteric heat of adsorption is about 60 kJ mol^{-1}, which suggests that physisorption takes place at the uncoordinated Cr sites. For larger coverages ($p/p^\circ > 0.1$), the heat of adsorption is 44–50 kJ mol^{-1}, which is slightly higher than the enthalpy of vaporization of water. These measurements support the assumption that, in MOF with pore size larger than 20 Å, adsorption proceeds through physisorption on cluster sites at low pressure while capillary condensation occurs at larger pressure.

The latter description of adsorption followed by capillary condensation in large pores is not a specific feature of MOFs. This is described in detail in ref. 30 and 35 which deal with other porous materials such as porous silicas and activated carbons. For MOF with pore size smaller than 20 Å, the mechanism of pore filling with water is largely unexplored and might be case dependent.[43] For CO_2 adsorption, Walton *et al.*

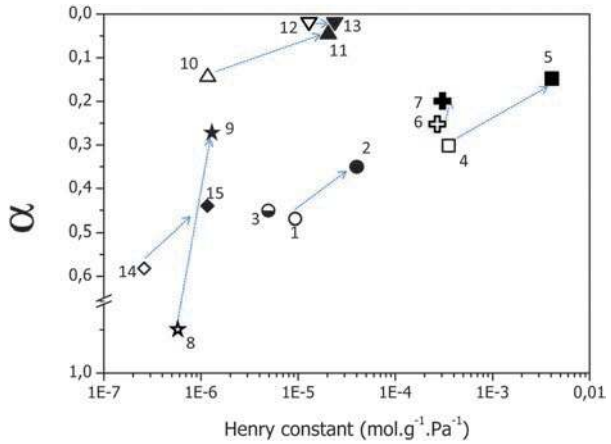

Fig. 8 Hydrophilicity–hydrophobicity map of MOF materials showing the filling pressure α as a function of Henry constant K_H. α corresponds to the pressure at which half of the water capacity C_{H_2O} is reached. K_H corresponds to the slope of the water adsorption isotherm measured for pressures $p/p^\circ < 0.1$. Open and close symbols correspond respectively to non-functionalized and functionalized materials (●: MIL-101, ■: UiO-66, ✚: MIL-125, ★: ZIF, ▲: Al-MIL-53, ▼: Ga-MIL-53, ◆: MIL-68).

have shown that, for the same MOF, adsorption can be of type I or type V depending on temperature.[44] Nevertheless, we assume that mechanisms shall be similar to those encountered in carbons. Surface water molecules first adsorb onto oxygenated–hydroxylated surface sites, and these adsorbed water molecules then act as nuclei for the formation of larger water clusters. Eventually, these clusters connect either along the surface or across the pore and pore filling occurs.[45] When the density of oxygenated sites on the surface is appreciable, pore filling occurs through a continuous filling process. UiO solids seem to follow the latter mechanism which is supported by larger heats of adsorption.[28]

A very small hysteresis was observed for most of the adsorption isotherms (even for microporous MOFs). We believe that the flexibility of the network, which is an intrinsic characteristic of MOF, is at the origin of this generally encountered phenomenon. While the Henry constant reflects mostly the surface chemistry, α (the pressure at which pore filling occurs) is rather linked to the pore size. However, as expected, significant correlations are observed between these two indicators (Fig. 8). Moreover if the eqn (1) is valid as an accurate guideline when comparing materials with different pore sizes, the data on Henry constants nevertheless show that this quantity also affects to some extent the capillary condensation pressure. Very low Henry constants are mostly associated with high α values while high Henry constants correspond to low α values. The functionalization of MOFs by polar groups (either amino or aldehyde) systematically leads to a shift of the Henry constant concomitant with a shift to lower α at the adsorption branch. This is consistent with the reduction of the apparent pore size at near pore filling or condensation pressure since the adsorbed water layers occupy part of the cavities. The results presented in Fig. 8 provide guidelines for the rational design of MOF adsorbents for heat-pump and chiller applications. The relative humidity α at which most of the water uptake occurs is a selection criterion for adsorbents. Indeed, adsorbents which fulfill the criterion $0.05 < \alpha < 0.32$ with an uptake larger than $0.2\ g\ g^{-1}$ are potential candidates. Obviously, the functionalisation of MOF enhances the adsorption properties towards this target.

5. Conclusion

Based on a library of 15 metal–organic frameworks exhibiting diverse pore size, topology and surface functions, we provide main guidelines for the design of MOFs with specific hydrophilicity–hydrophobicity properties. We show that the diversity in terms of hydrophilicity–hydrophobicity can be quantitatively described by three indicators which derive from water adsorption isotherms at room temperature: (1) the Henry constant, K_H, which corresponds to the slope of the adsorption isotherm at very low water partial pressures, (2) the relative pressure $\alpha = p/p^\circ$ at which half of the total water capacity is reached, and (3) the water adsorption capacity C_{H_2O}. The total water uptake C_{H_2O} is correlated with the porous volume at the exception of MOFs with gate opening properties and superhydrophobicity such as ZIF-8. The Henry constant K_H mainly describes the surface adsorption properties whereas the pressure α at which half of the uptake occurs mostly reflects the pore size although correlation exists between these two descriptors. Indeed, the functionalization of the frameworks by hydrophilic moieties such as hydrogen bonding groups (amine or aldehyde) systematically enhances surface hydrophilicity, as expressed by the Henry constant, which consecutively leads to a lower condensation/pore filling pressure α.

In the specific case of water at room temperature, the critical apparent pore diameter (D_c) which determines the mechanism of adsorption is expected to be around 20 Å. Every hysteresis loop observed for pores smaller than this critical value pertains to a different phenomenon than capillary condensation. In the present work, such non-capillary condensation hysteresis loops are attributed to framework flexibility or linker re-orientation upon adsorption–desorption. Beyond the adsorption mechanism and guidelines for the design of MOFs, we report a collection of adsorption isotherms of MOFs which can be relevant for applications. The "S" shaped adsorption isotherms are particularly of interest for heat-pumps and adsorbent-based chillers. Among such a library of water adsorption isotherms in MOFs, we report for the first time an extreme "S" shape isotherm for MIL-68 which is reversible.

Acknowledgements

We thank Dr Laurence Rozes (UPMC, Paris) for providing MIL-125 samples.

Notes and references

1 M. Soulard, J. Patarin, V. Eroshenko and R. Regis, in *Recent Advances in the Science and Technology of Zeolites and Related*

Materials, ed. E. VanSteen, M. Claeys and L. H. Callanan, 2004, vol. 154, pp. 1830–1837.

2 (*a*) A. C. Kizzie, A. G. Wong-Foy and A. J. Matzger, *Langmuir*, 2011, **27**, 6368–6373; (*b*) J. Liu, P. K. Thallapally, B. P. McGrail, D. R. Brown and J. Liu, *Chem. Soc. Rev.*, 2012, **41**, 2308–2322; (*c*) J. Liu, J. Tian, P. K. Thallapally and B. P. McGrail, *J. Phys. Chem. C*, 2012, **116**, 9575–9581.

3 E. Soubeyrand-Lenoir, C. Vagner, J. W. Yoon, P. Bazin, F. Ragon, Y. K. Hwang, C. Serre, J.-S. Chang and P. L. Llewellyn, *J. Am. Chem. Soc.*, 2012, **134**, 10174–10181.

4 A. O. Yazaydin, A. I. Benin, S. A. Faheem, P. Jakubczak, J. J. Low, R. R. Willis and R. Q. Snurr, *Chem. Mater.*, 2009, **21**, 1425–1430.

5 Y. F. Chen, R. Babarao, S. I. Sandler and J. W. Jiang, *Langmuir*, 2010, **26**, 8743–8750.

6 M. Sadakiyo, H. Okawa, A. Shigematsu, M. Ohba, T. Yamada and H. Kitagawa, *J. Am. Chem. Soc.*, 2012, **134**, 5472–5475.

7 (*a*) J. Janchen, D. Ackermann, H. Stach and W. Brosicke, *Sol. Energy*, 2004, **76**, 339–344; (*b*) G. Restuccia, A. Freni, F. Russo and S. Vasta, *Appl. Therm. Eng.*, 2005, **25**, 1419–1428; (*c*) E.-P. Ng and S. Mintova, *Microporous Mesoporous Mater.*, 2008, **114**, 1–26; (*d*) J. Bauer, R. Herrmann, W. Mittelbach and W. Schwieger, *Int. J. Energy Res.*, 2009, **33**, 1233–1249; (*e*) S. K. Henninger, H. A. Habib and C. Janiak, *J. Am. Chem. Soc.*, 2009, **131**, 2776–2777; (*f*) S. K. Henninger, F. P. Schmidt and H. M. Henning, *Appl. Therm. Eng.*, 2010, **30**, 1692–1702.

8 P. Kuesgens, M. Rose, I. Senkovska, H. Froede, A. Henschel, S. Siegle and S. Kaskel, *Microporous Mesoporous Mater.*, 2009, **120**, 325–330.

9 P. M. Schoenecker, C. G. Carson, H. Jasuja, C. J. J. Flemming and K. S. Walton, *Ind. Eng. Chem. Res.*, 2012, **51**, 6513–6519.

10 (*a*) T. Düren, Y.-S. Bae and R. Q. Snurr, *Chem. Soc. Rev.*, 2009, **38**, 1237–1247; (*b*) L. Sarkisov, T. Duren and R. Q. Snurr, *Mol. Phys.*, 2004, **102**, 211–221; (*c*) J. Canivet, A. Fateeva, Y. Guo, B. Coasne and D. Farrusseng, *Chem. Soc. Rev.*, 2014, submitted.

11 G. Akiyama, R. Matsuda, H. Sato, A. Hori, M. Takata and S. Kitagawa, *Microporous Mesoporous Mater.*, 2012, **157**, 89–93.

12 G. E. Cmarik, M. Kim, S. M. Cohen and K. S. Walton, *Langmuir*, 2012, **28**, 15606–15613.

13 C. R. Wade, T. Corrales-Sanchez, T. C. Narayan and M. Dinca, *Energy Environ. Sci.*, 2013, **6**, 2172–2177.

14 (*a*) C. Scherb, R. Koehn and T. Bein, *J. Mater. Chem.*, 2010, **20**, 3046–3051; (*b*) S. Biswas, T. Ahnfeldt and N. Stock, *Inorg. Chem.*, 2011, **50**, 9518–9526; (*c*) S. Biswas, T. Remy, S. Couck, D. Denysenko, G. Rampelberg, J. F. M. Denayer, D. Volkmer, C. Detavernier and P. Van Der Voort, *Phys. Chem. Chem. Phys.*, 2013, **15**, 3552–3561; (*d*) T. Fukushima, S. Horike, Y. Inubushi, K. Nakagawa, Y. Kubota, M. Takata and S. Kitagawa, *Angew. Chem., Int. Ed.*, 2010, **49**, 4820–4824.

15 H. Reinsch, M. A. van der Veen, B. Gil, B. Marszalek, T. Verbiest, D. de Vos and N. Stock, *Chem. Mater.*, 2013, **25**, 17–26.

16 (*a*) S. Bernt, V. Guillerm, C. Serre and N. Stock, *Chem. Commun.*, 2011, **47**, 2838–2840; (*b*) M. Hartmann and M. Fischer, *Microporous Mesoporous Mater.*, 2012, **164**, 38–43.

17 (*a*) M. Dan-Hardi, C. Serre, T. Frot, L. Rozes, G. Maurin, C. Sanchez and G. Ferey, *J. Am. Chem. Soc.*, 2009, **131**, 10857–10859; (*b*) C. H. Hendon, D. Tiana, M. Fontecave, C. Sanchez, L. D'Arras, C. Sassoye, L. Rozes, C. Mellot-Draznieks and A. Walsh, *J. Am. Chem. Soc.*, 2013, **135**, 10942–10945.

18 (*a*) J. H. Cavka, S. Jakobsen, U. Olsbye, N. Guillou, C. Lamberti, S. Bordiga and K. P. Lillerud, *J. Am. Chem. Soc.*, 2008, **130**, 13850–13851; (*b*) M. Kandiah, S. Usseglio, S. Svelle, U. Olsbye, K. P. Lillerud and M. Tilset, *J. Mater. Chem.*, 2010, **20**, 9848–9851.

19 (*a*) S. Aguado, J. Canivet and D. Farrusseng, *Chem. Commun.*, 2010, **46**, 7999–8001; (*b*) S. Aguado, J. Canivet and D. Farrusseng, *J. Mater. Chem.*, 2011, **21**, 7582–7588.

20 K. S. Park, Z. Ni, A. P. Cote, J. Y. Choi, R. Huang, F. J. Uribe-Romo, H. K. Chae, M. O'Keeffe and O. M. Yaghi, *Proc. Natl. Acad. Sci. U. S. A.*, 2006, **103**, 10186–10191.

21 C. Serre, F. Millange, C. Thouvenot, M. Nogues, G. Marsolier, D. Louer and G. Ferey, *J. Am. Chem. Soc.*, 2002, **124**, 13519–13526.

22 (*a*) S. Couck, J. F. M. Denayer, G. V. Baron, T. Remy, J. Gascon and F. Kapteijn, *J. Am. Chem. Soc.*, 2009, **131**, 6326–6327; (*b*) J. Gascon, U. Aktay, M. D. Hernandez-Alonso, G. P. M. van Klink and F. Kapteijn, *J. Catal.*, 2009, **261**, 75–87.

23 C. Volkringer, M. Meddouri, T. Loiseau, N. Guillou, J. Marrot, G. Ferey, M. Haouas, F. Taulelle, N. Audebrand and M. Latroche, *Inorg. Chem.*, 2008, **47**, 11892–11901.

24 M. Savonnet, D. Bazer-Bachi, N. Bats, J. Perez-Pellitero, E. Jeanneau, V. Lecocq, C. Pinel and D. Farrusseng, *J. Am. Chem. Soc.*, 2010, **132**, 4518–4519.

25 (*a*) C. Volkringer, T. Loiseau, N. Guillou, G. Ferey, E. Elkaim and A. Vimont, *Dalton Trans.*, 2009, 2241–2249; (*b*) U. Ravon, G. Chaplais, C. Chizallet, B. Seyyedi, F. Bonino, S. Bordiga, N. Bats and D. Farrusseng, *ChemCatChem*, 2010, **2**, 1235–1238.

26 P. L. Llewellyn, S. Bourrelly, C. Serre, Y. Filinchuk and G. Ferey, *Angew. Chem., Int. Ed.*, 2006, **45**, 7751–7754.

27 S. Aguado, J. Canivet, Y. Schuurman and D. Farrusseng, *J. Catal.*, 2011, **284**, 207–214.

28 (*a*) F. Jeremias, V. Lozan, S. K. Henninger and C. Janiak, *Dalton Trans.*, 2013, **42**, 15967–15973; (*b*) Y. Zhang, Y. Chen, Y. Zhang, H. Cong, B. Fu, S. Wen and S. Ruan, *J. Nanopart. Res.*, 2013, **15**, 1–6.

29 J. Ehrenmann, S. K. Henninger and C. Janiak, *Eur. J. Inorg. Chem.*, 2011, 471–474.

30 (*a*) B. Coasne, A. Galarneau, R. J. M. Pellenq and F. Di Renzo, *Chem. Soc. Rev.*, 2013, **42**, 4141–4171; (*b*) B. Coasne, K. E. Gubbins and R. J. M. Pellenq, *Adsorption*, 2005, **11**, 289–294.

31 (*a*) F.-X. Coudert, A. Boutin, A. H. Fuchs and A. V. Neimark, *J. Phys. Chem. Lett.*, 2013, **4**, 3198–3205; (*b*) A. U. Ortiz, A. Boutin, A. H. Fuchs and F.-X. Coudert, *Phys. Rev. Lett.*, 2012, 109.

32 S. Aguado, C.-H. Nicolas, V. Moizan-Basle, C. Nieto, H. Amrouche, N. Bats, N. Audebrand and D. Farrusseng, *New J. Chem.*, 2011, **35**, 41–44.

33 (*a*) E. Stavitski, E. A. Pidko, S. Couck, T. Remy, E. J. M. Hensen, B. M. Weckhuysen, J. Denayer, J. Gascon and F. Kapteijn,

Langmuir, 2011, **27**, 3970–3976; (*b*) T. Lescouet, E. Kockrick, G. Bergeret, M. Pera-Titus, S. Aguado and D. Farrusseng, *J. Mater. Chem.*, 2012, **22**, 10287–10293.

34 G. Chaplais, A. Simon-Masseron, F. Porcher, C. Lecomte, D. Bazer-Bachi, N. Bats and J. Patarina, *Phys. Chem. Chem. Phys.*, 2009, **11**, 5241–5245.

35 Y. Hanzawa and K. Kaneko, *Langmuir*, 1997, **13**, 5802–5804.

36 T. Loiseau, C. Serre, C. Huguenard, G. Fink, F. Taulelle, M. Henry, T. Bataille and G. Ferey, *Chem. – Eur. J.*, 2004, **10**, 1373–1382.

37 F. Rouquerol, J. Rouquerol and K. Sing, *Adsorption by Powders and Porous Solids: Principles, Methodology and Applications*, Academic, 1999.

38 B. Siboulet, B. Coasne, J.-F. Dufreche and P. Turq, *J. Phys. Chem. B*, 2011, **115**, 7881–7886.

39 (*a*) F. Cailliez, M. Trzpit, M. Soulard, I. Demachy, A. Boutin, J. Patarin and A. H. Fuchs, *Phys. Chem. Chem. Phys.*, 2008, **10**, 4817–4826; (*b*) N. Desbiens, I. Demachy, A. H. Fuchs, H. Kirsch-Rodeschini, M. Soulard and J. Patarin, *Angew. Chem., Int. Ed.*, 2005, **44**, 5310–5313.

40 (*a*) B. Coasne, A. Galarneau, F. Di Renzo and R. J. M. Pellenq, *Adsorption*, 2008, **14**, 215–221; (*b*) B. Coasne, A. Galarneau, F. Di Renzo and R. J. M. Pellenq, *J. Phys. Chem. C*, 2009, **113**, 1953–1962.

41 G. Akiyama, R. Matsuda and S. Kitagawa, *Chem. Lett.*, 2010, **39**, 360–361.

42 F. Jeremias, A. Khutia, S. K. Henninger and C. Janiak, *J. Mater. Chem.*, 2012, **22**, 10148–10151.

43 D. Fairen-Jimenez, N. A. Seaton and T. Duren, *Langmuir*, 2010, **26**, 14694–14699.

44 K. S. Walton, A. R. Millward, D. Dubbeldam, H. Frost, J. J. Low, O. M. Yaghi and R. Q. Snurr, *J. Am. Chem. Soc.*, 2008, **130**, 406–407.

45 (*a*) C. L. McCallum, T. J. Bandosz, S. C. McGrother, E. A. Muller and K. E. Gubbins, *Langmuir*, 1999, **15**, 533–544; (*b*) M. Thommes, C. Morlay, R. Ahmad and J. P. Joly, *Adsorption*, 2011, **17**, 653–661.